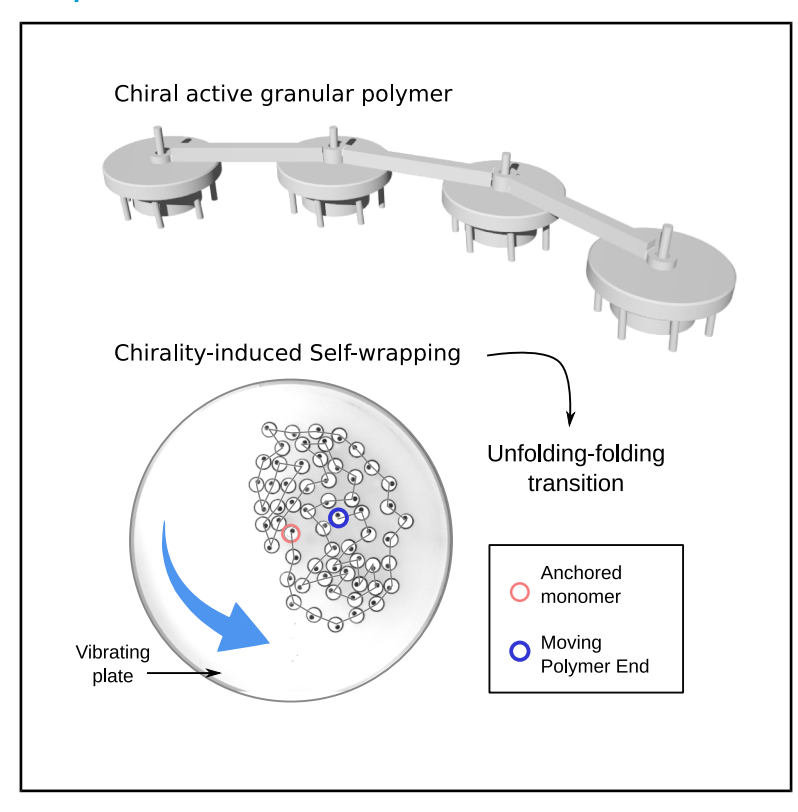
Newton

Spontaneous self-wrapping in chiral active polymers

Graphical abstract



Highlights

- Show spontaneous unfolded-folded transition in chiral active polymers
- Observe self-wrapping behavior in the polymer dynamics due to chiral activity
- Demonstrate anomalous Flory exponent in out-ofequilibrium polymers

Authors

Lorenzo Caprini, Iman Abdoli, Umberto Marini Bettolo Marconi, Hartmut Löwen

Correspondence

lorenzo.caprini@uniroma1.it

In brief

Chirality is a widely observed property in the physical and natural world. Caprini et al. discover that chirality spontaneously induces an unfolding-folding transition and generates self-wrapped configurations in active polymers, which are demonstrated via experiments with chains of chiral active granular particles and active Brownian simulations. The results challenge standard concepts in equilibrium polymer physics and pave the way for the exploration of chirality in active polymers at the intersection of soft matter and non-equilibrium statistical physics.



Newton



Article

Spontaneous self-wrapping in chiral active polymers

Lorenzo Caprini, 1,2,4,* Iman Abdoli, 1 Umberto Marini Bettolo Marconi, 3 and Hartmut Löwen 1

- ¹Institut für Theoretische Physik II: Weiche Materie, Heinrich-Heine-Universität Düsseldorf, 40225 Düsseldorf, Germany
- ²Physics Department, Sapienza University of Rome, Piazzale Aldo Moro 5, 00185 Rome, Italy
- ³Physics Department, University of Camerino, via Madonna delle Carceri, 62032 Camerino, Italy
- ⁴Lead contact

*Correspondence: lorenzo.caprini@uniroma1.it https://doi.org/10.1016/j.newton.2025.100253

ACCESSIBLE OVERVIEW Several animals, such as pangolins and armadillos, utilize rolling-up strategies to form self-wrapped configurations for defense against predators. Similarly, snakes and worms use these techniques to regulate body temperature and prevent desiccation. On a smaller scale, DNA wraps around proteins to form nucleosomes, which coil into chromatin structures, and proteins fold into coiled configurations. This study investigates this wrapping behavior by experimentally studying an active chain made of chiral active vibrobots, mimicking the aforementioned biologically inspired behavior. These vibrobots are an example of chiral active granular particles that move autonomously when placed on a vibrating plate. Self-wrapped configurations are observed when each fundamental polymer unit is chiral or, in other words, is characterized by the breaking of body rotational symmetry, leading to circular motion. This results in a spontaneous transition from unfolded to folded configurations uniquely induced by chiral activity. This phenomenon lacks an equilibrium counterpart and challenges current theories of equilibrium polymer physics, giving rise to anomalous Flory exponents. The discovery paves the way for developing innovative strategies for designing robots that can self-organize in rolled or unrolled configurations, with potential applications in swarm robotics.

SUMMARY

Biological organisms often have elongated, flexible structures with some degree of chirality in their bodies or movements. In nature, these organisms frequently take advantage of self-encapsulation mechanisms that create folded configurations, changing their functionality, such as for defensive purposes. Here, we explore the role of chirality in polymeric structures composed of chiral active monomers exhibiting circular motion. Through a combination of experiments and numerical simulations, we demonstrate a spontaneous unfolding-folding transition uniquely induced by chirality, a phenomenon not observed in passive polymers. This transition is driven by a self-wrapping mechanism, resulting in dynamic polymer collapse even without attractive interactions. Our findings, based on chiral polymers made from chiral active granular particles, present new opportunities in robotic applications, taking advantage of the interplay between chirality and deformability.

INTRODUCTION

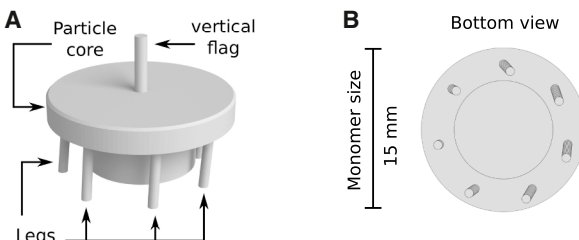
Chirality, the property of objects to be non-superimposable on their mirror images, is an ubiquitous property in science, specifically in physics, chemistry, and biology. From a fundamental perspective, chirality has been observed in particle physics: fermions and antifermions engaging in the charged weak interaction are left chiral and right chiral, respectively. Because of their coupling, it has been postulated that the entire universe is left-handed chiral. In chemistry, several molecules, such as the common sugar glucose, are characterized by an intrinsic

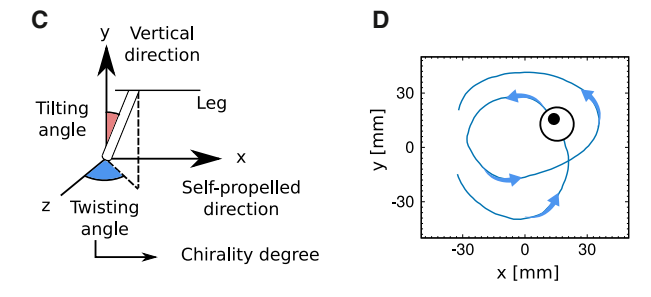
chirality. A similar scenario is encountered in biology (for instance, in amino acids and several cells), where chirality arises from the self-organization of the actin cytoskeleton.

In the realm of active-matter systems, ^{4–6} the interplay between particle motion and chirality has recently emerged as a captivating frontier offering insights into an array of fascinating phenomena. ⁷ Chirality introduces an intriguing twist to the dynamics of active particles, ⁸ leading to a unique class of emergent phenomena, ^{9–13} ranging from hyperuniform phases in dilute systems ^{14–16} to microphase separation ^{17–20} and self-reverting vorticity ²¹ in denser systems. The rotational symmetry breaking

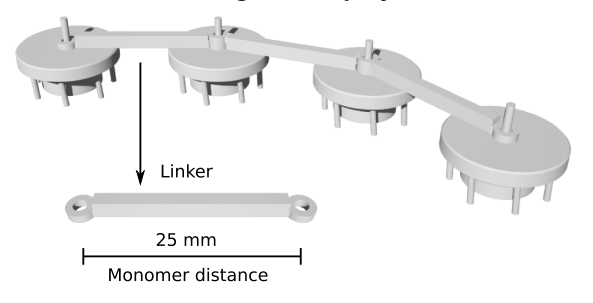


Chiral active granular particle





E Chiral active granular polymer



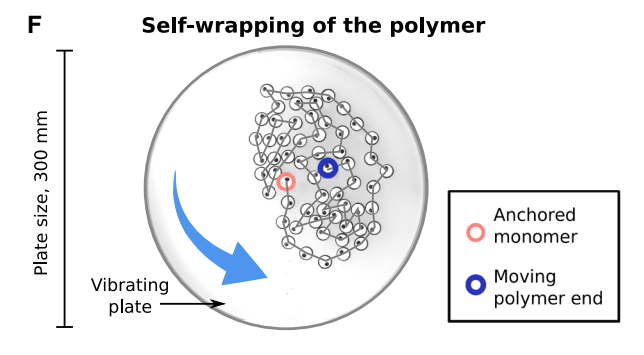


Figure 1. Chirality-induced self-wrapping and polymer folding

(A and B) 3D and bottom view of a chiral active granular particle.

- (C) Illustration of the leg design, showing both tilting and twisting angles.
- (D) Time trajectory of chiral active granular particles, showing circular motion.
- (E) Illustration of a chiral polymer consisting of chiral active granular particles kept together by a 3D-printed linker.
- (F) Folded configuration, showing a persistent rotation (blue arrow). The anchored monomer is marked in red, while the free-to-move polymer end is marked in blue.

due to chirality induces the emergence of odd properties, ²² such as odd elasticity, ^{23–26} odd viscosity, ^{27–29} and odd diffusivity, ^{30–32} which offer intriguing perspectives for the design of metamaterials. Chirality has been experimentally observed in biological active systems consisting of elongated flexible bodies, such as cytoskeleton filaments³³ and protofilaments in bacterial cells, ³⁴ while several bacteria themselves are chiral. ³⁵ Despite the huge theoretical work on active polymers ^{36–48} (i.e., filaments consisting of self-propelled particles), the role of chirality in these systems has been poorly explored.

Here, we discover a spontaneous folding transition in chiral active polymers; i.e., chain-like structures consisting of chiral active monomers that rotate with a constant angular velocity. This transition is powered by a self-wrapping mechanism that leads to spiral-like configurations characterized by a finite average winding number. The self-wrapping process occurs spontaneously without attraction or alignment interactions and is observed when each monomer self-rotates with a sufficiently large angular velocity. This phenomenon is responsible for polymer collapse despite the absence of attractive interactions between the fundamental polymer units. Our results are obtained via active granular experiments⁴⁹⁻⁵⁶ designed to include chirality. After fabricating chiral active granular particles (Figures 1A-1C), which exhibit circular trajectories (Figure 1C), we linked them together to create a chiral active granular polymer with a tunable structure. The experimental results presented here are supported by numerical simulations that elucidate the role of chirality as the primary mechanism driving the spontaneous folding transition.

Our findings highlight the crucial role of chirality in active polymers in self-organization phenomena. The self-wrapping mechanism paves the way for the design of autonomous soft, multi-component robots with a degree of deformability. Rotations in the single components of a robot may be employed to enhance the cohesivity of the whole robotic structure. These robotic agents may use self-wrapping in a biomimetic spirit, exploiting the rolling-up strategy of pangolins and armadillos to protect themselves against predators.

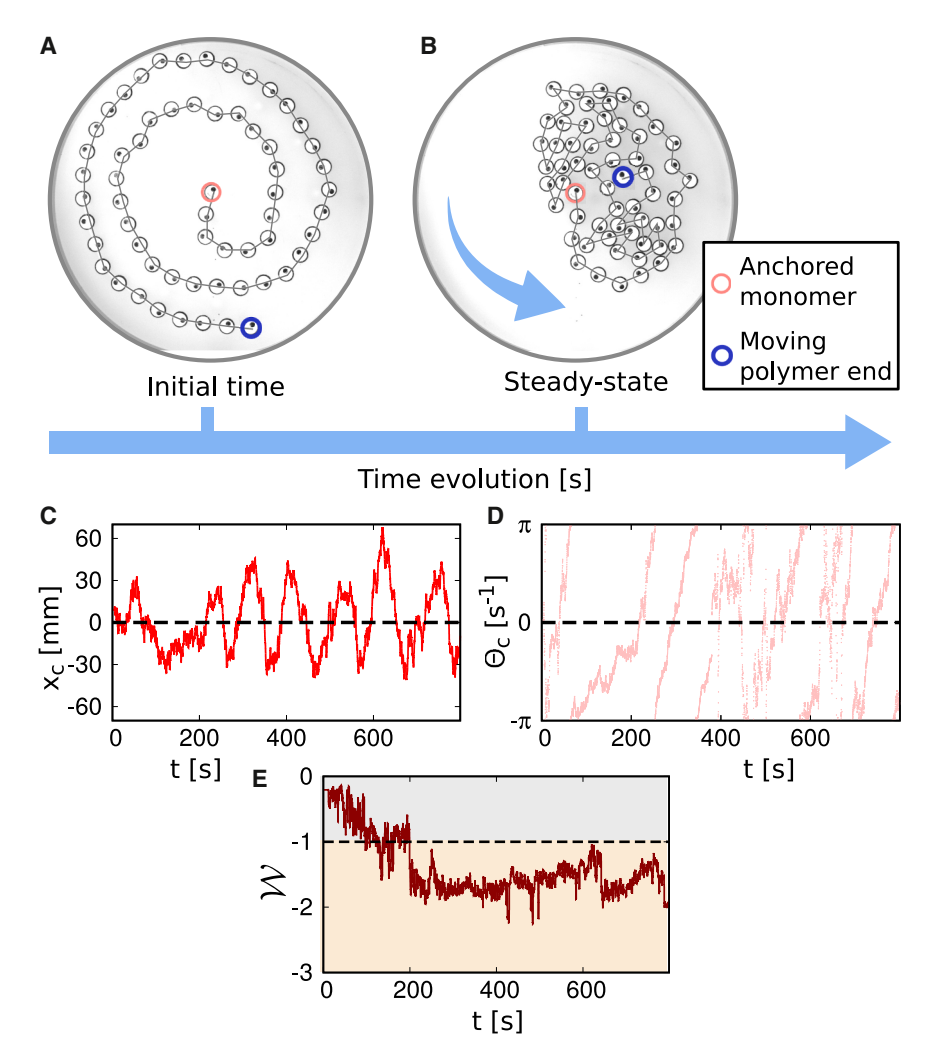
RESULTS

Chiral active granular particles

We design chiral active granular particles as 3D-printed plastic objects with broken translational and rotational symmetry. These particles possess a cylindrical body (Figure 1A) and multiple legs that contact a vibrating baseplate. Under vertical vibrations generated by an electromagnetic shaker, these particles exhibit stochastic motion, the characteristics of which depend on the design of their legs. ⁵⁷ Tilting all legs in the same direction induces direct self-propelled motion at speed v_0 for a typical duration, defining the particle persistence time, τ . Furthermore, twisting all legs either clockwise or counterclockwise disrupts rotational symmetry (Figures 1B and 1C), resulting in a self-rotating motion with a typical angular velocity, ω . This constant angular velocity, generated by a constant torque, will be referred to as chirality, as usual in the context of active matter. The superposition of these effects enables the granular particles to execute circular

Newton Article





trajectories (Figure 1D) with a typical radius $R \sim v_0/\omega$. Therefore, our objects behave as chiral active granular particles. Further details about the experimental setup are reported under methods, while single-particle chiral motion, including the mean-square displacement ^{58,59} and the diffusion coefficient, ^{58,60} are reported in Note S1 and Figures S1 and S2).

Chiral active granular polymers

An experimental realization of a chiral active polymer is realized by linking the centers of chiral active granular particles with a rigid rod capable of free rotations (Figure 1E). This configuration allows us to create a flexible chain of granular particles, each of which independently exhibits circular motion (see methods for further details). Here, the polymer is considered chiral because it consists of monomers that are all chiral in the same direction in such a way that the average chirality (average angular velocity) over the whole chain is not zero. To avoid collisions with the container's boundary in experiments, we anchor the end of the polymer to the center of the plate (Figures 2A and 2B). At first, we observe that our polymer behaves overall as an elongated structure with an intrinsic degree of chirality. This is evident by

Figure 2. Self-wrapping in spontaneous folded configurations

(A and B) Experimental snapshot configurations at the initial and final time. The red monomer is anchored to the middle of the plate, while the blue monomer is the free-to-move polymer head. The blue arrow denotes the polymer collective rotations around the plate center.

(C and D) Polymer center-of-mass position (X_c) (C) and angular position Θ_c (D) calculated from the center of the plate as a function of time t. Measurements are obtained for a polymer with N=60 monomers.

(E) Winding number \mathcal{W} relative to the free-to-move polymer head as a function of time t, showing the polymer self-wrapping. Here, a horizontal line marks the value -1 splitting configurations where the polymer head is self-trapped (yellow) and unrolled (gray).

monitoring the time trajectory of the whole polymer, which persistently rotates around the anchored monomer; the center-of-mass position, specifically the x component (x_c), shows time oscillations (Figure 2C), while the center-of-mass angular position Θ_c , from the center of the plate, increases from $-\pi$ to π as a function of time t (Figure 2D). This behavior can be explained by recognizing that the polymer's center of mass behaves as a chiral active particle with a non-zero average angular velocity.

Spontaneous polymer folding

Even starting from unrolled initial configurations with respect to the free-

to-move polymer head, the system spontaneously evolves toward a spontaneous folding state, where the polymer is permanently enrolled around its head (Figure 2B). This steady-state configuration is induced by a self-wrapping mechanism, observed both experimentally and numerically. In the folded configuration, the free-to-move polymer head is completely surrounded by other monomers, which effectively induces a self-trapping mechanism (Video S1). These surrounding monomers hinder the motion of the polymer head, preventing it from easily escaping and unfolding the polymer. Consequently, once this configuration is reached, the polymer can be considered to be in a metastable state. This behavior is confirmed for various polymer lengths (number of monomers N) and is independent of the initial configurations (Note S2; Figure S3). This effect is entirely due to chirality; the circular trajectories do not easily allow the monomers to find the correct path to unfold the polymer.

To quantify the self-wrapping mechanism, we study the winding number, \mathcal{W} , calculated on the free-to-move polymer head (Figure 2E). By describing the polymer as a continuous curve connecting the monomers, this observable counts the total



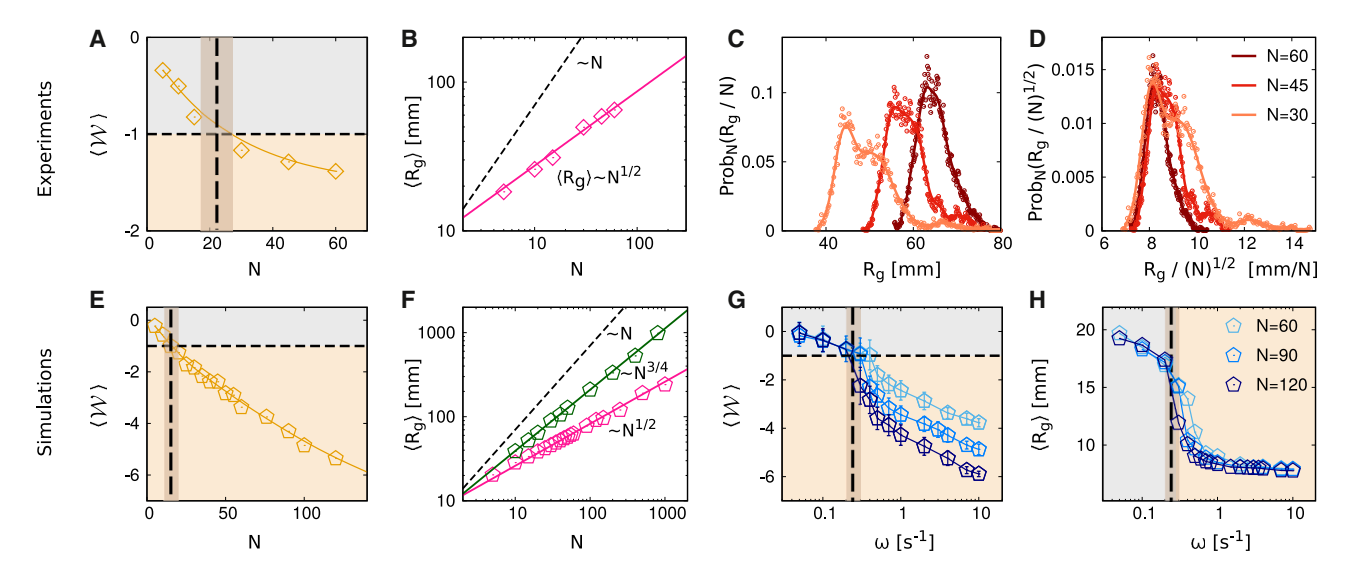


Figure 3. Chirality-induced unfolding-folding transition

(A and E) Average winding number $\langle \mathcal{W} \rangle$ as a function of the number of monomers N from experiments (A) and simulations (E). (B and F) Average gyration radius $\langle R_g \rangle$ as a function of N, from experiments (B) and simulations (F). In (F), pink dots are obtained under experimental conditions with chirality $\omega = 4 \text{ s}^{-1}$ and green dots with $\omega = 0.1 \text{ s}^{-1}$. Pink and green lines fit the functions $\sim N^{1/2}$ and $\sim N^{3/4}$, while dashed black lines show the $\sim N$ scaling.

(C) Probability distribution, $Prob(R_g)$, of the polymer gyration radius R_g .

(D) $\operatorname{Prob}(R_g)$ for the rescaled gyration radius R_g/N . Both (C) and (D) are obtained for N=60,45,30.

(G) $\langle \mathcal{W} \rangle$ as a function of the chirality ω .

(H) $\langle R_g \rangle$ as a function of ω .

(G) and (H) are calculated from simulations. Vertical dashed lines in (G) and (H) mark the critical value of ω where the folded-unfolded transition occurs. In (A)–(H), self-wrapping occurs if the winding number is smaller than -1 (yellow region). Errors in (A)–(H) are calculated from the standard deviation. When error bars are not present, these errors are smaller than the point size. The parameters of the simulations are reported in Tables 1 and 2.

number of loops performed around the polymer head (see methods for the definition of \mathcal{W}). At the initial time, when the polymer is unrolled with respect to the head, $\mathcal{W}(t) \approx 0$. After a transient period, $\mathcal{W}(t)$ reaches values smaller than -1, indicating that the polymer performs at least one loop around the head. In this case, self-wrapping is achieved, and the polymer reaches a folded configuration. This effect is not observed for $N \leq 15$, while it becomes stronger as N is increased until it approaches values close to -2 for N = 60. This is shown by studying the average winding number $\langle \mathcal{W} \rangle$ as a function of N (Figure 3A).

Chirality-induced unfolding-folding transition

The mechanism that leads to folded configurations is purely based on chirality. This idea is confirmed through simulations using a minimal model, consisting of a chiral active polymer with N monomers. Each monomer behaves as a chiral active granular particle, exhibiting underdamped active dynamics in the presence of chirality (methods). Linked monomers interact via a strong harmonic potential with a finite resting length, ensuring that the distance between them remains fixed. Additionally, excluded volume is modeled through a purely repulsive potential. Simulations qualitatively agree with experiments, showing that the average winding number $\langle W \rangle$ monotonically decreases with N, and selfwrapping is achieved for a polymer length $N \sim 20$ (Figure 3E). The quantitative discrepancy between experiments and simulations (smaller values of $\langle W \rangle$ for large N) can originate from dissipative effects during collisions or additional torques due to rotational friction in experiments. However, simulations show that these

interaction mechanisms are not crucial to observing self-wrapping.

Numerical simulations are used to investigate the main mechanism behind our experimental findings. Specifically, we observe that an increase in chirality ω induces a folding transition (Figure 3G), where we use the average winding number $\langle \mathcal{W} \rangle$ as an order parameter. For chirality values below a critical threshold $\omega < \omega_c$, $\langle W \rangle$ is close to zero, and the polymer remains unfolded (Video S2). For $\omega > \omega_c$, by contrast, $\langle W \rangle$ is smaller than -1, and the polymer reaches a folded configuration (Videos S3 and S4). This is confirmed by varying the polymer length by considering different numbers of monomers N. For small chirality, the polymer can easily disrupt a folded configuration because the head persistently moves in the same direction, pushing other monomers away. However, this disruption does not occur with large chirality, where the polymer head follows circular trajectories with a small radius, significantly reducing its effective persistence and thus its ability to push away other monomers.

Self-wrapping and polymer folding are observed only if all the monomers have the same chirality. This is checked in Note S5 and Figure S7, where we have numerically proven the absence of the folding transition if neighboring monomers have the same chirality magnitude with different signs. In this case, neighboring monomers tend to rotate in opposite directions, counteracting each other and suppressing self-wrapping. This implies that the folding transition is observed if the whole polymer is chiral, where the chirality of the polymer can be defined as the

Newton Article



average chirality over the chain of monomers. In addition, the spatial distribution of the monomers' chirality along the polymer chain matters; if a large block of monomers is characterized by the same clockwise (counterclockwise) chirality, then it is possible to also observe partial folding if the total chirality of the polymer is zero (Note S5; Figure S6).

To observe a long-time persistent folding, it is necessary that chirality—the angular velocity induced by a constant torque—does not reverse over time. As shown in Note S5 and Figure S6, if chirality is subject to stochastic dynamics able to turn clockwise chiral monomers into counterclockwise chiral monomers over time, then the folding transition is suppressed. However, if the changing rate of chirality is small, then the polymer may switch from a clockwise self-wrapped to a counterclockwise self-wrapped configuration passing through an unfolded state. This may cause the formation of tangles in an interacting system of chiral active polymers, as shown experimentally in the case of worms. ⁶¹

We remark that the mechanism leading to self-wrapping has some analogies to the mechanism responsible for enhanced clustering of passive particles in active baths. ⁶² Specifically, clusters of passive particles are stabilized when the turning rate of active particles on colliding with passive ones is large. This turning rate is set by the ratio of the interaction torque and viscous drag, while, in the present study, it is set by the ratio of the active torque to the substrate friction. However, while in Gokhale et al. ⁶² the handedness of the torque is unimportant, here, having monomers with the same chirality along the chain is a crucial ingredient.

Chirality-induced anomalous Flory exponent

To extract information about the polymer's internal structure, particularly its compactness, we measure the gyration radius, $R_g^2 = \sum_i |\mathbf{x}_i - \langle \mathbf{x} \rangle|^2$, where the average is taken over all monomers. In polymer physics, it is known that $\langle R_g \rangle$ scales with the number of monomers N following a power law $R_g \sim N^\nu$, where ν is called the Flory exponent. This exponent primarily depends on the system's dimensions, and, for passive polymers consisting of repulsive particles, it can be exactly calculated through the free energy minimization: in two dimensions, $\nu=3/4$.

The spontaneous folding observed experimentally results in a gyration radius governed by an anomalous Flory exponent, $\nu \approx$ 1/2, despite the presence of excluded volume effects; i.e., pure repulsion between different monomers. This information has been derived from calculating the steady-state average $\langle R_a \rangle$ (Figure 3B) and the distribution of the gyration radius, $Prob(R_q)$ (Figure 3C). Indeed, the distribution $Prob(R_q)$ obtained for different N collapses by rescaling $\langle R_g \rangle \rightarrow R_g/N^{1/2}$ (Figure 3D). This result is confirmed by numerical simulations where the exponent $\nu = 1/2$ is measured for larger polymer lengths N (pink data in Figure 3F). The change of the Flory exponent from $\nu = 3/4$ (passive value) to $\nu = 1/2$ (chiral active value) is uniquely induced by chirality. This is numerically checked by considering an active polymer with low chirality where the folding transition is not observed and, consequently, $\nu \approx 3/4$ (green data in Figure 3F). We note that $\nu = 1/2$ in two dimensions is consistent with the collapse exponent, confirming the spontaneous folding observed in both experiments and simulations. As a result, the average gyration radius can be used as an alternative order parameter to quantify the chirality-induced folding transition. Indeed, $\langle R_g \rangle$ as a function of ω displays a sudden jump from large values where the polymer is unfolded to a plateau value that is close to the minimal length compatible with a folded configuration (Figure 3E).

Effective attractions governing chiral active polymers

Simulations with a non-anchored polymer in a box with periodic boundary conditions demonstrate that the self-wrapping is not due to the polymer anchoring. In this case, self-wrapping can be quantified by calculating the average winding number $\langle \mathcal{W} \rangle$ defined by Equation 8. By symmetry, half of the polymer self-wraps around the head and half around the tail, displaying two spiral-like configurations in the same (clockwise) direction (Figure 4A), similar to Anand (see also Note S3 and Figure S4). This implies that self-wrapping is more difficult to achieve for a non-anchored polymer; the required N is twice the one observed in the anchored case.

By systematically varying the polymer length (i.e., the number of monomers N) and the chirality ω (other parameters are chosen from experiments; see Table 2), we confirm the scenario shown in Figure 3G. The folding transition is achieved for $N \gtrsim 30$ (corresponding to $N \gtrsim 15$ for a non-anchored polymer) for a critical value ω_c which is almost constant with N (Figure 4B). Indeed, the polymer length, NL, should be large enough to allow the polymer to self-wrap. This requires that NL is larger than the typical radius of the circular trajectory v_0/ω so that $N \gtrsim N_c = v_0/(\omega L)$ (or, equivalently, $\omega > v_0/(NL)$). This condition is satisfied in experiments where $N_c \approx 1$, and, thus, self-wrapping always occurs if there are enough monomers to surround the polymer head. The threshold value in ω arises from a different mechanism; self-wrapping occurs when the radius of the circular trajectory v_0/ω is smaller than the persistence length of the active force $v_0\tau$, where $\tau = 1/D_r$. This implies that the folding transition can be observed for $\omega > 1/\tau$ (dashed black line in Figure 4). This scaling law is numerically confirmed in Figure 4C (dashed black line) in the plane of ω and τ at fixed N. This scaling stops to hold for low values of ω when the condition $\omega > v_0/(NL)$ is not satisfied (red dashed line).

To theoretically explain the polymer collapse, observed experimentally and numerically, we derive the effective interactions governing the dynamics of non-linked monomers. Specifically, we consider an effective equilibrium approach originally derived by Fox⁶⁵ and recently applied to non-chiral active matter.^{66,67} Here, the method is applied to chiral active particles (see Note S6 for the derivation) and maps the interplay between chiral activity and repulsive forces due to steric interactions on an effective potential, $V_{eff}(r)$, with an attractive part (see Equation S35 for the final prediction). Indeed, the persistent motion typical of chiral active objects allows them to remain stuck to each other for a typical persistence time as if the two particles were kept together by weak attractive interactions. In our chiral active polymer, these effective attractive forces mainly rule the dynamics of distant monomers. Indeed, neighboring monomers are kept at a constant distance by the potential Ulink. By contrast, monomers placed far apart in the polymer chain are not directly linked and can move persistently against each other. Consequently,



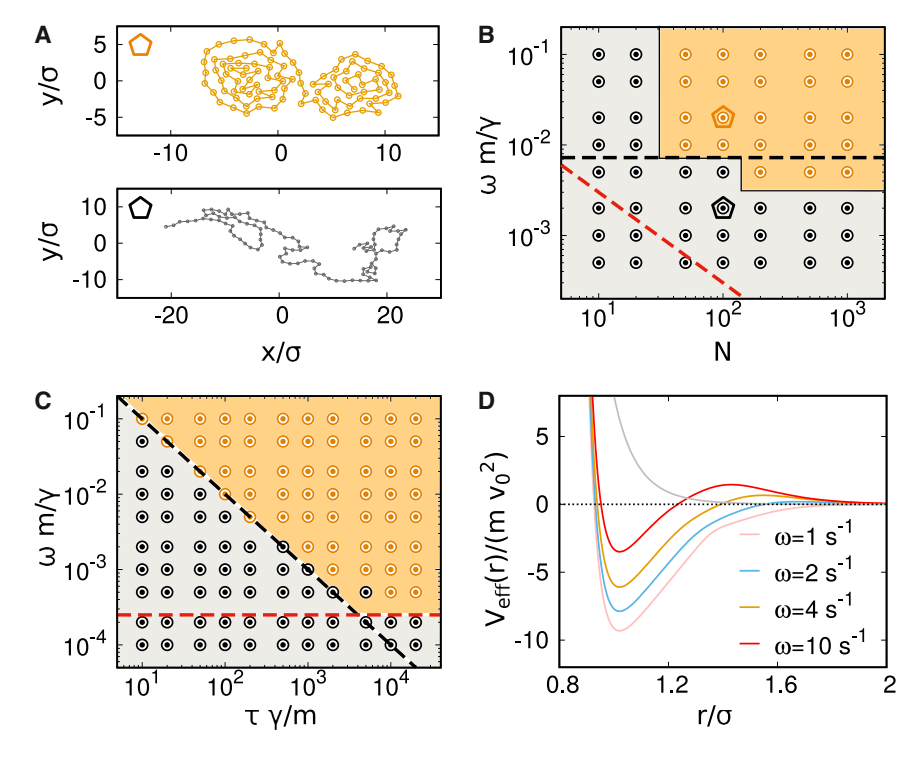


Figure 4. Phase diagrams for nonanchored polymers and effective attraction

(A) Self-wrapped and open configurations for a non-anchored polymer numerically explored with N = 100.

(B and C) State diagrams displaying self-wrapping (yellow) or open configurations (gray), where (B) shows the state diagram in the plane of chirality ω and number of monomers N (with fixed $\tau=1/D_r=1.4$), and (C) shows it in the plane of ω and persistence time $\tau=1/D_r$ (with fixed N=100). Time is normalized with the inertial time m/γ . In both diagrams, the dashed black line reports the curves $\omega=1/\tau$, while the dashed red line reports the curves $\omega=v_0/(NL)$. Yellow and gray pentagons in (B) correspond to the configurations reported in (A).

(D) Effective potential $V_{\rm eff}(r)$ governing the dynamics of chiral active particles for different values of the chirality ω . Effective potential is derived in Equation S35 and is normalized by the typical energy scale of inertial active particles $\sim mv_0^2$. The gray line denotes the repulsive potential $\sim 1/r^{12}$. The parameters to perform simulations and plot Equation S33 are reported under methods (Tables 1 and 2).

they are subject to the effective attractive interactions predicted theoretically. This effective attraction survives for a broad range of chirality values (Figure 4D) in the experimental conditions of our chiral active monomers and, thus, provides a qualitative, effective explanation for the polymer folding transition. As a result, this prediction explains the 1/2 Flory exponent observed experimentally and numerically for large chirality. Indeed, this exponent is the one that can be measured for a generic collapsed polymer; for instance, a passive one where distant monomers attract each other.

DISCUSSION

Here, the interplay between chirality and body flexibility is investigated by experimentally studying a granular polymer consisting of chiral active particles. We discover that chirality significantly alters the polymer's conformational properties, leading to a spontaneous folding that has no equilibrium counterpart, as supported by numerical simulations. This result is induced by a self-wrapping mechanism that leads to spiral-like configurations and represents a spontaneous dynamical collective phenomenon generated by the independent rotations of each monomer. The intrinsic chirality often found in natural polymer units can explain the folding of proteins or biological filaments as well as self-encapsulation mechanisms for defense purposes.

A similar self-wrapping effect and folding transition can be observed for a chiral (eccentric) active polymer evolving in three dimensions. On one hand, we expect that the dimensionality increase hinders the folding transition, which may require larger chirality values to be observed. On the other hand, the self-wrapped configurations could promote enhanced entanglement

effects. Indeed, the rotating motion of each monomer could promote expected knotting phenomena compared to the passive or non-chiral counterparts. In addition, our theory also applies in three dimensions and for vanishing chirality. Therefore, it can qualitatively explain the globular or compressed configurations typically observed in polymers subject to tangential activity. 38,68

The experimental folding transition is reproduced numerically by simulating a chiral active polymer with a fully flexible structure. This means that chiral active monomers only interact through excluded volume effects and forces between neighboring particles, which keeps the monomer distance fixed. Since the linkers connecting the monomers are free to rotate, this fully flexible structure reproduces our experimental results, and we do not need to include a bending stiffness contribution; i.e., a potential force that quantifies how resistant an elongated structure is to bending. This additional force, which typically characterizes semi-flexible polymers, favors elongated configurations. Consequently, its primary effect is to suppress the folding transition (see Note S4 and Figure S5 for further details on this numerical study). However, for intermediate values of the bending stiffness, we observe partial folding; the monomers close to the anchored one remain preferentially in elongated configurations while the remaining monomers self-wrap around the free-to-move polymer head. Beyond these preliminary results, we expect that chiral active semi-flexible polymers may reveal intriguing conformations and collective phenomena in future studies.

Our results challenge the conventional polymer theories applicable in equilibrium, showing that anomalous values of the Flory exponent can arise spontaneously as a non-equilibrium effect. The presence of chiral activity drives the polymer far from equilibrium and allows us to observe folded polymer

Newton Article



configurations even without attractions. The self-wrapping phenomenon observed experimentally and numerically is a general property of polymers characterized by rotating units, here obtained by considering monomers with chiral dynamics. Similar self-wrapping phenomena can be potentially realized in polymers where rotations are induced by magnetic fields, with potential applications in swarm robotics, where each unit has a degree of flexibility and is sensitive to magnetic forces.

METHODS

Experimental setup

To conduct our experiment, we employed a standard vibrating table, a well-established tool for inducing vibrational excitations in granular materials. Our setup comprises an acrylic baseplate with a diameter of 300 mm and a height of 15 mm, complemented by an outer plastic ring that confines the particles within. Vertical vibrations are generated by an electromagnetic shaker affixed to the acrylic baseplate. Horizontal alignment was meticulously adjusted to minimize the influence of gravitational drift. Additionally, we placed the setup on a substantial concrete block to counteract resonance effects with the environment. Our choice of shaker frequency f and amplitude A was critical for achieving stable excitation without particle spillage. We operated at f = 120 Hz with an amplitude of $A = 24(1)\mu m$, ensuring quasi-2D particle motion on the baseplate.

Active chiral particle design

The particles used in our study are 3D plastic objects created through 3D printing.⁶⁹ Each particle possesses cylindrical symmetry and consists of a main body with multiple laterally attached legs. The particle body is composed of two primary components: (1) a cylindrical core with a diameter of 9 mm and a height of 4 mm, designed to stabilize the particle by lowering its center of mass vertically, and (2) a larger cylindrical cap with a diameter of 15 mm and a height of 2 mm, which defines the particle's circular horizontal cross-section. This cap serves as the attachment point for seven cylindrical legs, each with a diameter of 0.8 mm. These legs are distributed regularly around the core, forming a heptagonal configuration. The legs make contact with the ground, resulting in a total particle height of 7 mm, with a vertical leg height of 5 mm, and the core is suspended 4 mm above the ground. On average, each particle has a mass of m = 0.83 g, and its moment of inertia, determined by the particle's shape, is $J = 17.9 \text{ g mm}^2$.

To induce self-propelled motion, we introduce a disruption of the particle's translational symmetry by tilting all legs at a constant angle, α , in the same direction. This angle governs the particle's polarization and is indicated by a white spot attached to the particle's cap. A larger α corresponds to a higher typical particle velocity. We set α to 4° relative to the surface normal. Self-rotational motion is achieved by perturbing the cylindrical symmetry of the particle's legs. In this case, all legs are additionally twisted at the same angle of 3.4° relative to the vertical, in the counterclockwise direction (so that the particle rotates counterclockwise). A larger twisting angle results in a higher particle angular velocity and, thus, circular trajectories with a smaller radius. Circular motion is attained by simulta-

neously tilting and twisting the legs, combining translational and rotational symmetry-breaking mechanisms.

Dynamics of a chiral active granular particle

We characterize the dynamics of particles through a parametric approach based on modeling their motion using stochastic models for the particle dynamics. Specifically, the particle dynamics are described by the inertial active Brownian particle model, which encompasses underdamped dynamics for translational and rotational motion, which are coupled by the particle activity. The translational motion of an active vibrobot with mass m, position \mathbf{x} , and velocity $\mathbf{v} = \dot{\mathbf{x}}$ is well-represented by a 2D stochastic differential equation that balances inertial, dissipative, and active forces⁷⁰:

$$m\dot{\mathbf{v}} + \gamma \mathbf{v} = \gamma \sqrt{2D_t} \boldsymbol{\xi} + \gamma v_0 \mathbf{n}$$
 (Equation 1)

Here, ξ is Gaussian white noise with zero average and unit variance, while γ and D_t describe the friction and the effective translational diffusion coefficients, respectively. The active driving force is defined by $\gamma v_0 \mathbf{n}$, where v_0 represents the typical speed value, and $\mathbf{n} = (\cos\theta, \sin\theta)$ is the orientation vector calculated from the orientational angle θ .

The rotational dynamics of a particle, characterized by its moment of inertia J, is governed by an additional equation of motion for the angular velocity $\Omega = \dot{\theta}$:

$$J\dot{\Omega} = -\gamma_r \Omega + \gamma_r \sqrt{2D_r} \eta + \gamma_r \omega$$
. (Equation 2)

Here, η represents Gaussian white noise with zero average and unit variance, and γ_r and D_r are the rotational friction and rotational diffusion coefficients, respectively. Finally, the angular drift ω determines the particle chirality and represents the typical angular velocity of the chiral active particle.

Chiral active polymer design

Our chiral active particles feature a vertical central bar with a diameter of 1 mm, which resembles a slender rod. These bars are designed to facilitate the connection of two or more chiral active granular particles. This connection is achieved using 3D-printed rods, approximately 22 mm long, with a thickness and height of 3 mm. These plastic linkers are perforated at their ends, allowing them to be inserted into the vertical bars; the internal hole of these linkers has a radius of 2 mm. By connecting two chiral active granular particles, we can form a dimer. Connecting two or more dimers enables the creation of a polymer consisting of *N* monomers.

Dynamics of a chiral active polymer

With this setup, the friction between slender rods and particles is negligible, allowing the link to be effectively approximated solely as an interparticle force. This implies that the orientation of each monomer can be described Equation 2 without any torque interactions. By contrast, the translational dynamics of the center of mass of each monomer are governed by Equation 3 with an additional interaction force \mathbf{F}_i , so that

$$m\dot{\mathbf{v}}_i + \gamma \mathbf{v}_i = \gamma \sqrt{2D_t} \boldsymbol{\xi}_i + \gamma v_0 \mathbf{n}_i + \mathbf{F}_i,$$
 (Equation 3)





Table 1. Interaction parameters

Parameter	Parameter value
σ	15 mm
L	22 mm
k	$10^3 \mathrm{g} \mathrm{mm}^2 \mathrm{s}^{-2}$
ϵ	$1 \mathrm{~g~mm^2~s^{-2}}$

with i=1,...,N. The interparticle force is obtained by an interaction potential $\mathbf{F}_i=-\nabla_i U_{tot}$, which models the volume exclusion effect between different particles and the fixed distance between the particle centers:

$$U_{tot} = U_{ex} + U_{link}$$
. (Equation 4)

Here, the exclusion is modeled by the potential

$$U_{\text{ex}} = \sum_{i < i}^{N} U_{\text{WCA}},$$
 (Equation 5)

where U_{WCA} is the Weeks-Chandler-Andersen potential given by

$$U_{WCA} = 4\epsilon \left(\left(\frac{\sigma}{r} \right)^{12} - \left(\frac{\sigma}{r} \right)^{6} \right)$$
. (Equation 6)

The parameter σ represents the particle diameter, while ε determines the energy scale of the repulsion. The inter-monomer links are modeled by the following potential:

$$U_{link} = \frac{k}{2\sigma^2} \sum_{i=1}^{N-1} (|\mathbf{x}_{i+1} - \mathbf{x}_i| - L)^2,$$
 (Equation 7)

where L is the distance between neighboring monomers and k the constant of this potential. The parameters' value is reported in Table 1.

The dynamics of an anchored polymer are obtained by fixing the tail position to the origin and the dynamics of a non-anchored polymer by evolving all monomers in a box with periodic boundary conditions.

Estimate of the particle parameters

The interaction potentials' parameters are selected to ensure that σ represents the nominal particle diameter and to prevent large distance fluctuations between connected monomers. In contrast, the intrinsic parameters of the individual chiral active particle are determined using a fitting algorithm that assesses translational and angular velocity distributions, mean-squared displacement, and mean angular displacement. Experimental outcomes are compared with simulation results obtained from Equations 2 and 3, iteratively adjusting parameters such as v_0 , γ , γ_r , D_t , and ω . Initially, these observables are evaluated with a predefined parameter set. Subsequently, a Nelder-Mead optimization scheme is employed to minimize the overall deviation from the experimental data, iteratively searching for the optimal parameter set. Our estimate of the model parameters is reported in Table 2.

We observe that, at the shaker conditions considered, the persistence time $1/D_r=1.4~{\rm s}$ is larger than the other typical

Table 2. Parameters of a single chiral active particleParameterParameter value v_0 $56 (4) \text{ mm s}^{-1}$ γ $27 (2) \text{ g s}^{-1}$ D_t $3.7 (0.2) \text{ mm}^2 \text{ s}^{-1}$

 D_r 0.71 (0.01) s⁻¹ ω 3.98 (0.05) s⁻¹ γ_r 244 (30) g mm² s⁻¹.

times governing the dynamics; i.e., the chiral time $1/\omega=0.25$ s, the inertial time $m/\gamma=0.030$ s and the rotational inertial time $J/\gamma_r=0.73$ s. Therefore, inertia does not play a fundamental role in the dynamics of our experimental chiral active particles.

Winding number calculation

To calculate the number of complete rotations the polymer makes around the free-to-move monomer (head), we introduce a winding number, \mathcal{W} , as follows (Figure 5): (1) we calculate the unwrapped angle β_j formed between the horizontal axis and the vector linking the generic monomer j and the polymer head (marked in blue in Figure 5), and (2) we calculate the difference between consecutive angles without encountering discontinuity issues, since angles are unwrapped.

For a polymer with N monomers and assuming that the polymer head is identified as the monomer with j=1, the winding number \mathcal{W} is defined by summing the angles β_j formed by all remaining monomers (j>1) so that

$$W = \frac{1}{2\pi} \sum_{j=2}^{N-1} (\beta_{j+1} - \beta_j)$$
. (Equation 8)

With this definition, a positive winding number is measured when the polymer is wrapped counterclockwise around the polymer head, while a negative winding number is obtained when the polymer is wrapped clockwise. Since the angles β_j are unwrapped, ${\cal W}$ can assume values larger than 1, which account for more than one round around the polymer head. Finally, the 2π normalization allows us to identify ${\cal W}$ as the number of clockwise or counterclockwise rounds around the polymer head.

RESOURCE AVAILABILITY

Lead contact

Requests for further information and resources should be directed to and will be fulfilled by the lead contact, Lorenzo Caprini (lorenzo.caprini@uniroma1.it).

Materials availability

This study did not generate new materials.

Data and code availability

- Experimental and numerical data have been deposited in the online Zenodo repository and are publicly available as of the date of publication at https://zenodo.org/uploads/15105172. All other data reported in this paper will be shared by the lead contact upon request.
- All original code has been deposited at Zenodo (https://zenodo.org/ uploads/15105172) and is publicly available as of the date of

8





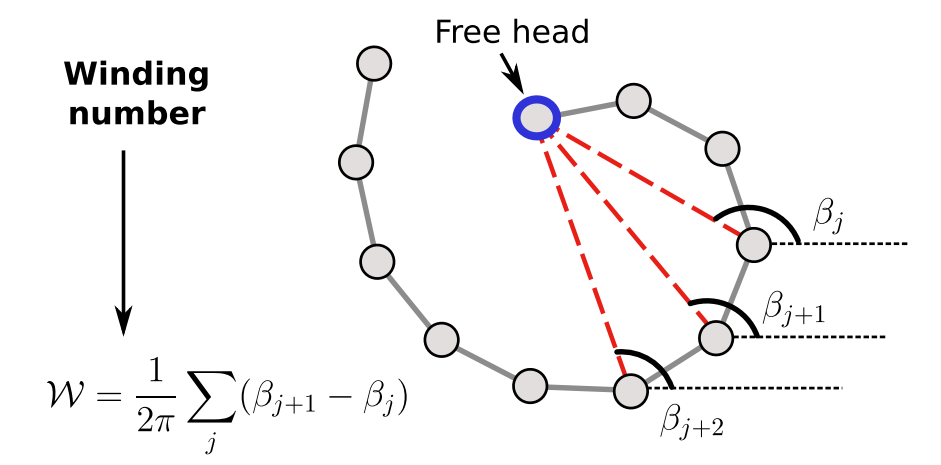


Figure 5. Winding number

The illustration shows the definition of the winding number, \mathcal{W} , with respect to the free-to-move polymer head (marked in blue). \mathcal{W} is calculated by summing the unwrapped angles β_j formed by the horizontal axis (black dashed line) and the distance between the monomer j and the polymer head (red dashed line).

publication. A file to reproduce the design of chiral active granular particles forming the chiral polymer is available online at https://zenodo.org/uploads/15105172.

 Any additional information required to reanalyze the data and data supporting the plots within this paper is available from the corresponding author upon request.

ACKNOWLEDGMENTS

L.C. and H.L. thank Olivier Dauchot for useful discussions. L.C. acknowledges the European Union MSCA-IF fellowship for funding the project CHIAGRAM and acknowledges funding from the Italian Ministero dell'Universitá e della Ricerca under the program PRIN 2022 ("re-ranking of the final lists"), number 2022KWTEB7, cup B53C24006470006. I.A. and H.L. acknowledge support from the Deutsche Forschungsgemeinschaft (DFG) through the SPP 2265, grant 418/25.

AUTHOR CONTRIBUTIONS

L.C., U.M.B.M., and H.L. conceived the project. L.C. designed and performed the experiment. I.A. and L.C. performed the experimental analysis and performed numerical simulations. L.C. wrote the first draft of the paper, but all authors contributed equally to manuscript writing.

DECLARATION OF INTERESTS

The authors declare no competing interests.

SUPPLEMENTAL INFORMATION

Supplemental information can be found online at https://doi.org/10.1016/j.newton.2025.100253.

Received: March 29, 2025 Revised: July 1, 2025 Accepted: September 3, 2025

REFERENCES

- 1. Prelog, V. (1976). Chirality in chemistry. Science 193, 17-24.
- Xu, J., Van Keymeulen, A., Wakida, N.M., Carlton, P., Berns, M.W., and Bourne, H.R. (2007). Polarity reveals intrinsic cell chirality. Proc. Natl. Acad. Sci. USA 104, 9296–9300.

- Tee, Y.H., Shemesh, T., Thiagarajan, V., Hariadi, R.F., Anderson, K.L., Page, C., Volkmann, N., Hanein, D., Sivaramakrishnan, S., Kozlov, M.M., and Bershadsky, A.D. (2015). Cellular chirality arising from the self-organization of the actin cytoskeleton. Nat. Cell Biol. 17, 445–457.
- Marchetti, M.C., Joanny, J.F., Ramaswamy, S., Liverpool, T.B., Prost, J., Rao, M., and Simha, R.A. (2013). Hydrodynamics of soft active matter. Rev. Mod. Phys. 85, 1143–1189.
- Elgeti, J., Winkler, R.G., and Gompper, G. (2015). Physics of microswimmerssingle particle motion and collective behavior: a review. Rep. Prog. Phys. 78, 056601.
- Bechinger, C., Di Leonardo, R., Löwen, H., Reichhardt, C., Volpe, G., and Volpe, G. (2016). Active particles in complex and crowded environments. Rev. Mod. Phys. 88, 045006.
- 7. Liebchen, B., and Levis, D. (2022). Chiral active matter. Europhys. Lett. 139, 67001.
- Löwen, H. (2016). Chirality in microswimmer motion: From circle swimmers to active turbulence. Eur. Phys. J. Spec. Top. 225, 2319–2331.
- Zhang, B., Sokolov, A., and Snezhko, A. (2020). Reconfigurable emergent patterns in active chiral fluids. Nat. Commun. 11, 4401.
- Siebers, F., Jayaram, A., Blümler, P., and Speck, T. (2023). Exploiting compositional disorder in collectives of light-driven circle walkers. Sci. Adv. 9, eadf5443.
- Liao, G.J., and Klapp, S.H.L. (2021). Emergent vortices and phase separation in systems of chiral active particles with dipolar interactions. Soft Matter 17, 6833–6847.
- 12. Ceron, S., OKeeffe, K., and Petersen, K. (2023). Diverse behaviors in non-uniform chiral and non-chiral swarmalators. Nat. Commun. 14, 940.
- Caprini, L., Löwen, H., and Marini Bettolo Marconi, U. (2023). Chiral active matter in external potentials. Soft Matter 19, 6234–6246.
- Lei, Q.L., Ciamarra, M.P., and Ni, R. (2019). Nonequilibrium strongly hyperuniform fluids of circle active particles with large local density fluctuations. Sci. Adv. 5, eaau7423.
- Huang, M., Hu, W., Yang, S., Liu, Q.X., and Zhang, H.P. (2021). Circular swimming motility and disordered hyperuniform state in an algae system. Proc. Natl. Acad. Sci. USA 118, e2100493118.
- Zhang, B., and Snezhko, A. (2022). Hyperuniform active chiral fluids with tunable internal structure. Phys. Rev. Lett. 128, 218002.
- Liebchen, B., and Levis, D. (2017). Collective behavior of chiral active matter: Pattern formation and enhanced flocking. Phys. Rev. Lett. 119, 058002
- Ma, Z., Lei, Q.I., and Ni, R. (2017). Driving dynamic colloidal assembly using eccentric self-propelled colloids. Soft Matter 13, 8940–8946.





- Ma, Z., and Ni, R. (2022). Dynamical clustering interrupts motility-induced phase separation in chiral active brownian particles. J. Chem. Phys. 156, 021102.
- Semwal, V., Joshi, J., Dikshit, S., and Mishra, S. (2024). Macro to micro phase separation of chiral active swimmers. Phys. A: Stat. Mech. Appl. 634, 129435.
- Caprini, L., Liebchen, B., and Löwen, H. (2024). Self-reverting vortices in chiral active matter. Commun. Phys. 7, 153.
- Fruchart, M., Scheibner, C., and Vitelli, V. (2023). Odd viscosity and odd elasticity. Annu. Rev. Condens. Matter Phys. 14, 471–510.
- Braverman, L., Scheibner, C., VanSaders, B., and Vitelli, V. (2021).
 Topological defects in solids with odd elasticity. Phys. Rev. Lett. 127, 268001.
- Kole, S.J., Alexander, G.P., Ramaswamy, S., and Maitra, A. (2021).
 Layered chiral active matter: Beyond odd elasticity. Phys. Rev. Lett. 126, 34213949.
- Tan, T.H., Mietke, A., Li, J., Chen, Y., Higinbotham, H., Foster, P.J., Gokhale, S., Dunkel, J., and Fakhri, N. (2022). Odd dynamics of living chiral crystals. Nature 607, 287–293.
- Bertoldi, K., Vitelli, V., Christensen, J., and Van Hecke, M. (2017). Flexible mechanical metamaterials. Nat. Rev. Mater. 2, 17066.
- Banerjee, D., Souslov, A., Abanov, A.G., and Vitelli, V. (2017). Odd viscosity in chiral active fluids. Nat. Commun. 8, 1573.
- Markovich, T., and Lubensky, T.C. (2021). Odd viscosity in active matter: microscopic origin and 3d effects. Phys. Rev. Lett. 127, 048001.
- Lou, X., Yang, Q., Ding, Y., Liu, P., Chen, K., Zhou, X., Ye, F., Podgornik, R., and Yang, M. (2022). Odd viscosity-induced hall-like transport of an active chiral fluid. Proc. Natl. Acad. Sci. USA 119, e2201279119.
- **30**. Hargus, C., Epstein, J.M., and Mandadapu, K.K. (2021). Odd diffusivity of chiral random motion. Phys. Rev. Lett. *127*, 178001.
- Kalz, E., Vuijk, H.D., Abdoli, I., Sommer, J.U., Löwen, H., and Sharma, A. (2022). Collisions enhance self-diffusion in odd-diffusive systems. Phys. Rev. Lett. 129, 090601.
- Muzzeddu, P.L., Vuijk, H.D., Löwen, H., Sommer, J.U., and Sharma, A. (2022). Active chiral molecules in activity gradients. J. Chem. Phys. 157, 134902.
- Dunajova, Z., Mateu, B.P., Radler, P., Lim, K., Brandis, D., Velicky, P., Danzl, J.G., Wong, R.W., Elgeti, J., Hannezo, E., and Loose, M. (2023). Chiral and nematic phases of flexible active filaments. Nat. Phys. 19, 1916–1926.
- Shi, H., Quint, D.A., Grason, G.M., Gopinathan, A., and Huang, K.C. (2020).
 Chiral twisting in a bacterial cytoskeletal polymer affects filament size and orientation. Nat. Commun. 11, 1408.
- Woolley, D.M. (2003). Motility of spermatozoa at surfaces. REPRODUC-TION-CAMBRIDGE- 126, 259–270.
- Winkler, R.G., Elgeti, J., and Gompper, G. (2017). Active polymersemergent conformational and dynamical properties: A brief review. J. Phys. Soc. Jpn. 86, 101014.
- Anand, S.K., and Singh, S.P. (2018). Structure and dynamics of a self-propelled semiflexible filament. Phys. Rev. E 98, 042501.
- Bianco, V., Locatelli, E., and Malgaretti, P. (2018). Globulelike conformation and enhanced diffusion of active polymers. Phys. Rev. Lett. 121, 217902
- Anand, S.K., and Singh, S.P. (2020). Conformation and dynamics of a selfavoiding active flexible polymer. Phys. Rev. E 101, 030501.
- Deblais, A., Maggs, A.C., Bonn, D., and Woutersen, S. (2020). Phase separation by entanglement of active polymerlike worms. Phys. Rev. Lett. 124, 208006.
- Vliegenthart, G.A., Ravichandran, A., Ripoll, M., Auth, T., and Gompper, G. (2020). Filamentous active matter: Band formation, bending, buckling, and defects. Sci. Adv. 6, eaaw9975.

- 42. Kurzthaler, C., Mandal, S., Bhattacharjee, T., Löwen, H., Datta, S.S., and Stone, H.A. (2021). A geometric criterion for the optimal spreading of active polymers in porous media. Nat. Commun. 12, 7088.
- Fazelzadeh, M., Irani, E., Mokhtari, Z., and Jabbari-Farouji, S. (2023).
 Effects of inertia on conformation and dynamics of tangentially driven active filaments. Phys. Rev. E 108, 024606.
- Faluweki, M.K., Cammann, J., Mazza, M.G., and Goehring, L. (2023).
 Active spaghetti: collective organization in cyanobacteria. Phys. Rev. Lett. 131, 158303.
- Janzen, G., and Matoz-Fernandez, D. (2024). Density and inertia effects on two-dimensional active semiflexible filament suspensions. Preprint at arXiv. https://doi.org/10.48550/arXiv:2405.06592.
- Fazelzadeh, M., Di, Q., Irani, E., Mokhtari, Z., and Jabbari-Farouji, S. (2023). Active motion of tangentially driven polymers in periodic array of obstacles. J. Chem. Phys. 159, 224903.
- Abbaspour, L., Malek, A., Karpitschka, S., and Klumpp, S. (2023). Effects of direction reversals on patterns of active filaments. Phys. Rev. Res. 5, 013171.
- Muzzeddu, P.L., Gambassi, A., Sommer, J.U., and Sharma, A. (2024).
 Migration and separation of polymers in nonuniform active baths. Phys. Rev. Lett. 133, 118102.
- Aranson, I.S., Volfson, D., and Tsimring, L.S. (2007). Swirling motion in a system of vibrated elongated particles. Phys. Rev. E 75, 051301.
- Kumar, N., Soni, H., Ramaswamy, S., and Sood, A.K. (2014). Flocking at a distance in active granular matter. Nat. Commun. 5, 4688.
- Scholz, C., Engel, M., and Pöschel, T. (2018). Rotating robots move collectively and self-organize. Nat. Commun. 9, 931.
- Koumakis, N., Gnoli, A., Maggi, C., Puglisi, A., and Leonardo, R.D. (2016).
 Mechanism of self-propulsion in 3d-printed active granular particles. New J. Phys. 18, 113046.
- Baconnier, P., Shohat, D., López, C.H., Coulais, C., Démery, V., Düring, G., and Dauchot, O. (2022). Selective and collective actuation in active solids. Nat. Phys. 18, 1234–1239.
- 54. López-Castaño, M.A., Márquez Seco, A., Márquez Seco, A., Rodríguez-Rivas, Á., and Reyes, F.V. (2022). Chirality transitions in a system of active flat spinners. Phys. Rev. Res. 4, 033230.
- 55. Xu, T.I., Qin, C.r., Tang, B., Gao, J.c., Zhou, J., Chen, K., Zhang, T.H., and Tian, W.d. (2024). Constrained motion of self-propelling eccentric disks linked by a spring. Preprint at arXiv. https://doi.org/10.48550/arXiv:2407.20610.
- Caprini, L., Ldov, A., Gupta, R.K., Ellenberg, H., Wittmann, R., Löwen, H., and Scholz, C. (2024). Emergent memory from tapping collisions in active granular matter. Commun. Phys. 7, 52.
- Antonov, A.P., Caprini, L., Ldov, A., Scholz, C., and Löwen, H. (2024). Inertial active matter with coulomb friction. Phys. Rev. Lett. 133, 198301.
- Van Teeffelen, S., and Löwen, H. (2008). Dynamics of a brownian circle swimmer. Phys. Rev. E 78, 020101.
- Reichhardt, C., and Reichhardt, C.J.O. (2019). Active microrheology, hall effect, and jamming in chiral fluids. Phys. Rev. E 100, 012604.
- Caprini, L., and Marini Bettolo Marconi, U. (2019). Active chiral particles under confinement: Surface currents and bulk accumulation phenomena. Soft Matter 15, 2627–2637.
- Patil, V.P., Tuazon, H., Kaufman, E., Chakrabortty, T., Qin, D., Dunkel, J., and Bhamla, M.S. (2023). Ultrafast reversible self-assembly of living tangled matter. Science 380, 392–398.
- 62. Gokhale, S., Li, J., Solon, A., Gore, J., and Fakhri, N. (2022). Dynamic clustering of passive colloids in dense suspensions of motile bacteria. Phys. Rev. E 105, 054605.
- De Gennes, P.G. (1979). Scaling Concepts in Polymer Physics (Cornell university press).
- **64.** Anand, S.K. (2025). Spiral folding of a flexible chain of chiral active particles. J. Phys. Condens. Matter *37*, 185101.
- Fox, R.F. (1986). Functional-calculus approach to stochastic differential equations. Phys. Rev. 33, 467–476.

Please cite this article in press as: Caprini et al., Spontaneous self-wrapping in chiral active polymers, Newton (2025), https://doi.org/10.1016/j. newton.2025.100253

Newton Article



- 66. Wittmann, R., Maggi, C., Sharma, A., Scacchi, A., Brader, J.M., and Marini Bettolo Marconi, U. (2017). Effective equilibrium states in the colored-noise model for active matter i. pairwise forces in the fox and unified colored noise approximations. J. Stat. Mech. 2017, 113207
- Wittmann, R., Smallenburg, F., and Brader, J.M. (2019). Pressure, surface tension, and curvature in active systems: A touch of equilibrium. J. Chem. Phys. 150, 174908.
- **68.** Winkler, R.G., and Gompper, G. (2020). The physics of active polymers and filaments. J. Chem. Phys. *153*, 040901.
- Caprini, L., Breoni, D., Ldov, A., Scholz, C., and Löwen, H. (2024). Dynamical clustering and wetting phenomena in inertial active matter. Commun. Phys. 7, 343.
- 70. Scholz, C., Jahanshahi, S., Ldov, A., and Löwen, H. (2018). Inertial delay of self-propelled particles. Nat. Commun. 9, 5156.